# Kinetics and Thermodynamics of Adsorption of Rhodamine B onto Bentonite Supported Nanoscale Zerovalent Iron Nanocomposite



# Kinetics and Thermodynamics of Adsorption of Rhodamine B onto Bentonite Supported Nanoscale Zerovalent Iron Nanocomposite

**Adewumi O. Dada[1]*, Folahan. A. Adekola[2], Ezekiel. O. Odebunmi[3], Adejumoke. A. Inyinbor[1], Banjo A Akinyemi[4], Ilesanmi, D. Adesewa[1]**

*[1]Industrial Chemistry Programme, Department of Physical Sciences, (Science and Technology Research Cluster), Landmark University, P.M.B.1001, Omu-Aran, Kwara State, Nigeria
[2]Department of Industrial Chemistry, University of Ilorin, P.M.B. 1515, Ilorin, Nigeria
[3]Department of Chemistry, University of Ilorin, P.M.B. 1515, Ilorin, Nigeria
[4]Farm Structures and Environment Unit, Department of Agricultural and Biosystems Engineering, Nigeria

*Corresponding author's e-mail: dada.oluwasogo@lmu.edu.ng

**Abstract**. Bentonite clay supported nanoscale zerovalent iron (BC-nZVI) composite was successfully prepared. BC-nZVI was characterized by physicochemical and spectroscopic techniques. Surface area as determined by sear's method is 291.2 $cm^2$. Adsorption operational parameters were investigated in a batch technique. At 500 mg/L initial concentration, 120 minutes contact time and pH 3, 454.81 mg/g quantity was adsorbed. The highest adsorption percentage removal efficiency was obtained at room temperature. Kinetic data fitted best to pseudo second order and the mechanism was diffusion governed. The kinetic models were further validated by sum of square error (SSE) and non-linear Chi-square statistical models ($X^2$). The values of the thermodynamic parameters: standard enthalpy change ΔH (-10.597 $Jmol^{-1}$)to (-5558 $Jmol^{-1}$.), standard entropy change, ΔS (-277.804 J $mol^{-1}$ $K^{-1}$)- to (-139.2595 J $mol^{-1}$ $K^{-1}$) and the Gibbs free energy (ΔG) revealed that the adsorption process was feasible, spontaneous and exothermic in nature. The performance of BC-nZVI enlisted it as a great potential adsorbent for effective removal of Rhodamine B and therefore recommended for application in industrial effluent treatment.

Keywords: Bentonite clay; Iron nanocomposite; Dyes; Kinetics; Mechanisms; Thermodynamics

## 1. Introduction

Assurance of environmental sustainability in the millennium development goals cannot be secured if the developing world is still battling with access to clean and unpolluted water. Due to higher demand for textile materials, greater production and use of synthetic dyes, all over the world, dye wastewater has become a major problem [1]. After production, most dye effluent from textile industries get into the water bodies and environment, and dyes have been found to escape convectional water treatment [2]. Based on unregulated and unguided discharge of effluents [3], dye molecules have found their route into the water bodies thereby rendering it unsafe and hazardous both to man and even the aquatic organisms. Not only do dyes impact colour on substances, they also travels with have high level of sulphates, phenolic compounds, lead, manganese etc. [4]. Rhodamine B is the dye under investigation in this research. It is a cationic dye commonly used in textile

industry due to its good fastness to fabrics and high solubility. However, it has been reported to be carcinogenic [5-6]. Thus, its removal from the environment becomes imperative.

There are a number of conventional methods of dyes removal nevertheless adsorption has been signposted to be cheap and efficient technique [7]. From literature, it was observed that efficacy of adsorption process depends on active and efficient adsorbent. Nanoparticles and its composite materials have been identified recently as adsorbents of unique characteristics and capacity for remediation. Although, a number of biomass and nanoadsorbents have been used for uptake of Rhodamine B dye. Few among those adsorbents are hydrothermal synthesized nanorods [8]; BiOBr/montmorillonite composites [9], Magnetic nanocomposite [10]; NiO nanoparticles [11]. However, BC-nZVI for Rhodamine B uptake has not been reported. Hence this work looks into the kinetics and thermodynamics of adsorption of Rhodamine B dye using BC-nZVI. This study will help in the design and construction of waste water and effluent treatment reactor.

## 2. Materials and Method

### 2.1. Reagents and Apparatus

Throughout this study, analytical grade reagents were used. Iron (III) chloride ($FeCl_3$) (Eurostar scientific, Liverpool, Uk), sodium borohydride ($NaBH_4$) (Qualikum, India), Ethanol (BDH Analar, 95% UN No 1997) was used without further purification. Vacuum filtration setup, 0.45 μm Millipore, Bentonite clay, distilled-deionized water, Rhodamine B (RhB).

### 2.2 Preparation of Bentonite Clay Supported Nanoscale Zerovalent Iron (BC-nZVI)

The base biomass used as one of the precursors in the preparation of BC-nZVI is bentonite. This was cleaned and spread in the laboratory overnight under open air and further oven dried at 105 $^{o}$C for 12 hr. The bentonite clay was separated using 150 μm sieve to increase the surface area. Thereafter, Bentonite clay Supported Zero-valent Composite was prepared on the account of our previous studies [12-15]. BC-nZVI was prepared following the simplified method;

STEP 1: 1 g of accurately weighed Bentonite Clay (BC) was added to a solution of 0.023 M $FeCl_3$ (3.73 g into 1000 mL deionized water) and stirred on a magnetic stirrer (model: J.W Towers) for 2 hrs to ensure homogeneity of the mixture of the two precursors.

STEP 2: 0.125 M $NaBH_4$ was transferred into the mixture of BC and $FeCl_3$ solution from step 1. This was followed by a fast stirring of the mixture for one hour until the whole of $NaBH_4$ solution was added. Homogeneous stirring was effected using magnetic stirrer in order to allow the BC percolate into the matrix of zerovalent iron nanoparticles (nZVI). A resulting black Bentonite Clay supported Nanoscale Zerovalent Iron (BC-nZVI) was formed and was separated using 0.4 μm Millipore filter paper on a vacuum filtration setup. BC-nZVI was further washed severally with ethanol to prevent rapid oxidation of zerovalent iron. The BC-nZVI was then dried at 50 $^{o}$C overnight and kept for further experimental work. BC-nZVI was used for adsorption studies vis-à-vis kinetics and thermodynamics. Post adsorption characterization was carried out via FTIR

### 2.3. Preparation of RhB Adsorbate Solution

1000 ppm RhB was prepared by dissolving a carefully weighed 0.1 g RhB in 1000 mL standard volumetric flask using distilled-deionized water. Lower concentrations (100 – 500 ppm) of freshly prepared RhB adsorbate were prepared by serial dilution.

### 2.4 Batch Kinetic with Validity and Thermodynamics Studies

Synergy was studied via time and concentration variation. At 100 mg BC-nZVI was contacted with different concentrations from 100 – 500 ppm at different contact time specifically 10 – 120 minutes. At optimum conditions, effect of temperature was studies at 25, 35, 45 and 55 $^{o}$C. Measurement of residual concentration of RhB was done at maximum wavelength using double beam Biochrom Ultraviolent Visible Spectrophotometer (UV-Vis). The quantity of Rhodamine B adsorbed on BC-nZVI at different time interval was determined using mass balance expression in Eq. 1 and the removal efficiency calculated using Eq. 2 as shown [15 – 16]:

$$q_t = \frac{(C_o - C_t)V}{W} \tag{1}$$

$$\%\ RE = \left(\frac{C_o - C_e}{C_o}\right) \times 100 \tag{2}$$

Kinetics, mechanisms and thermodynamics data obtained were tested using Eq. 3 – 9 [13, 14, 17]:

Pseudo first-order: $\log(q_e - q_t) = \log q_e - \frac{k_1 t}{2.303}$ (3)

Pseudo second-order: $\frac{t}{q_t} = \frac{1}{k_2 q_e^2} + \frac{1}{q_e} t$ (4)

Intraparticle Diffusion: $q_t = k_{id} t^{0.5} + C$ (5)

Liquid Film Diffusion: $\ln(1 - F) = -k_P t$ (6)

Where $F = {[q]_t^n}/{[q]_e^n}$ (7)

Van't Hoff: $\ln Kc = \frac{\Delta S}{R} - \frac{\Delta H}{RT}$ (8)

Where $Kc = \frac{Qe}{Ce}$ (9)

The kinetic models were eventually validated using Eq 10 – 11:

$$SSE = \sum_{i=1}^{n} \left(q_{e,cal} - q_{e,\exp}\right)^2 \tag{10}$$

$$\chi^2 = \sum_{i=1}^{n} \frac{\left(q_{e,\exp} - q_{e,cal}\right)^2}{q_{e,cal}} \tag{11}$$

## 3. Results and Discussion

### 3.1. Synergistic Effect of Contact time and Initial RhB Concentration and

Fig. 1 shows the synergistic effect of both contact time and initial concentration from 100 – 500 ppm at interval of 10 – 120 minutes. A rapid kinetics was observed at initial time of 10 minutes and later decreased as the time increases with increase in the driving force arising from the concentrations. The equilibrium time increased from 10 to 120 minutes with increase in concentration. Identified increase in the quantity adsorbed from 92.39 mg/g

to 495.95 mg/g maybe ascribed to increase in active adsorptive site and driving force as a result of mass transfer generated by RhB concentration [18-19]

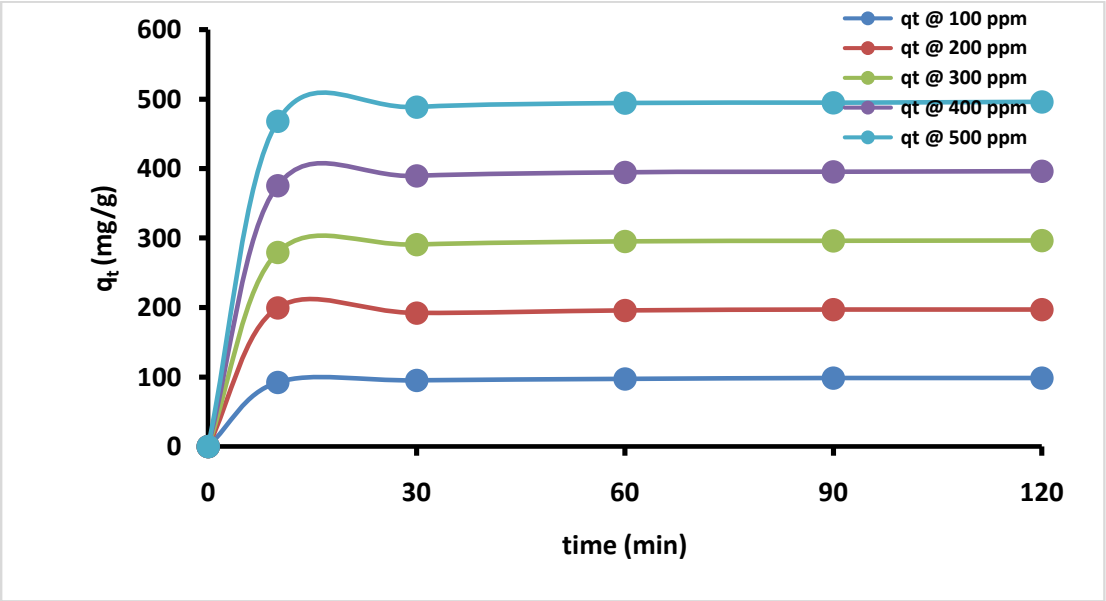


Fig. 1: Contact time at different Initial Concentration on RhB uptake

### 3.2. Adsorption Kinetics and Mechanisms of Sorption of RhB onto BC–nZVI Nanocomposite

Kinetic data were analyzed to determine the mechanisms and the rate of adsorption. Kinetics and mechanism models in Eq. 3-7 were utilized to describe the rapid process of uptake of RhB onto BC-nZVI. Calculated values of Pseudo first and second-order were obtained from the slope and intercept of the linear plots represented in Figs 2(A–B). Based on evaluated parameters, pseudo second-order better described the kinetics having $R^{2-}$ ranging from0.99 to 1. On the other hand, the $R^2$ values for pseudo first-order for all the concentrations showed that the kinetic data were badly represented. Considering other evaluated parameter such as rate constants ($k_1$ and $k_2$) and initial adsorption rate ($h_1$ and $h_2$) as presented in the Table 1. The higher adsorption rate from pseudo-second order was an indication of a fast adsorption process. There is a good agreement between the experimental quantity adsorbed and the calculated quantity adsorbed from pseudo second-order model. The statistical tools used for the validity of the model are sum of square error (SSE) and chi-square ($\chi^2$). Hence, this is attributed with high values of $R^2$, lower values of SSE and $\chi^2$ together with nearness amid values of $q_{e,exp}$ and $q_{e,\,cal}$[20 – 21].

Definite steps required to determine the mechanism are intraparticle/pore diffusion and Liquid film/surface diffusion. Fig. 3(A) shows the linear plots of intraparticle diffusion models. Straight line plot of $q_t$ against $t^{0.5}$with $R^2$ value relatively higher than 0.7 across investigated concentrations suggested that kinetic the data fitted to the model. Evaluated parameters revealed increase in the thickness as concentration increases indicating that boundary layers contribute to adsorption process. However, intraparticle diffusion plot not passing through the origin suggests that it is not the only rate determining factor, hence the mechanism is surface dependent.

Surface diffusion model also known as the Liquid diffusion as expressed in Eqs.6-7 [22]. It is the mechanism dealing with the transportation of RhB to the surface of BC-nZVI. The $R^2$ value of liquid film diffusion (Fig 3B)

being greater than 0.95 at the highest concentration (500 ppm) and also higher than that of intraparticle diffusion supports that adsorption process was surface and external diffusion dominant [12, 15, 22].

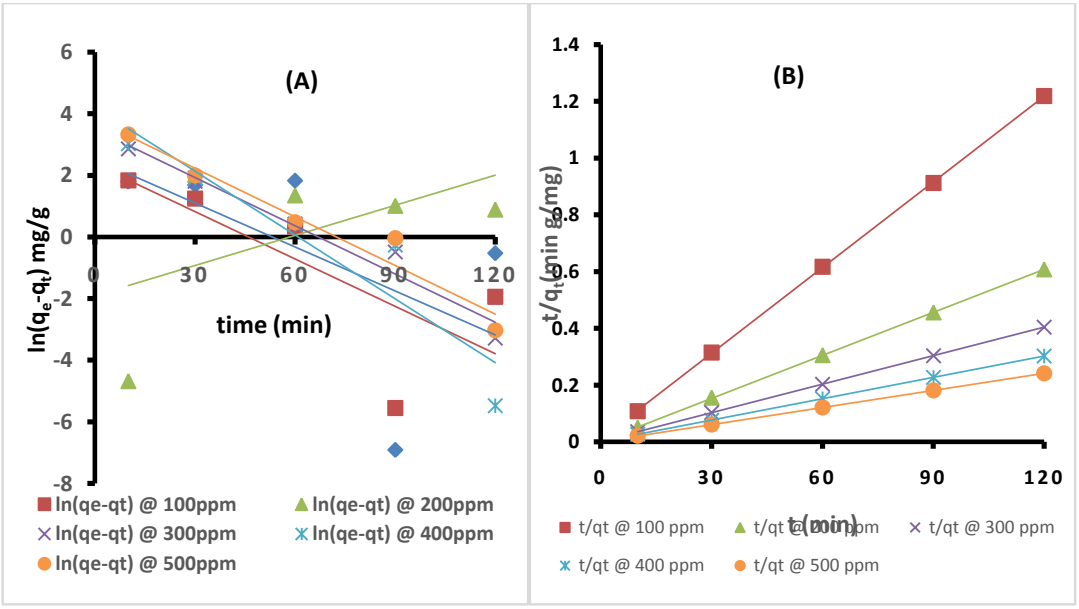


Fig 2: (A) Pseudo first-order (B) Pseudo second-order plot for adsorption of RhB onto B-nZVI

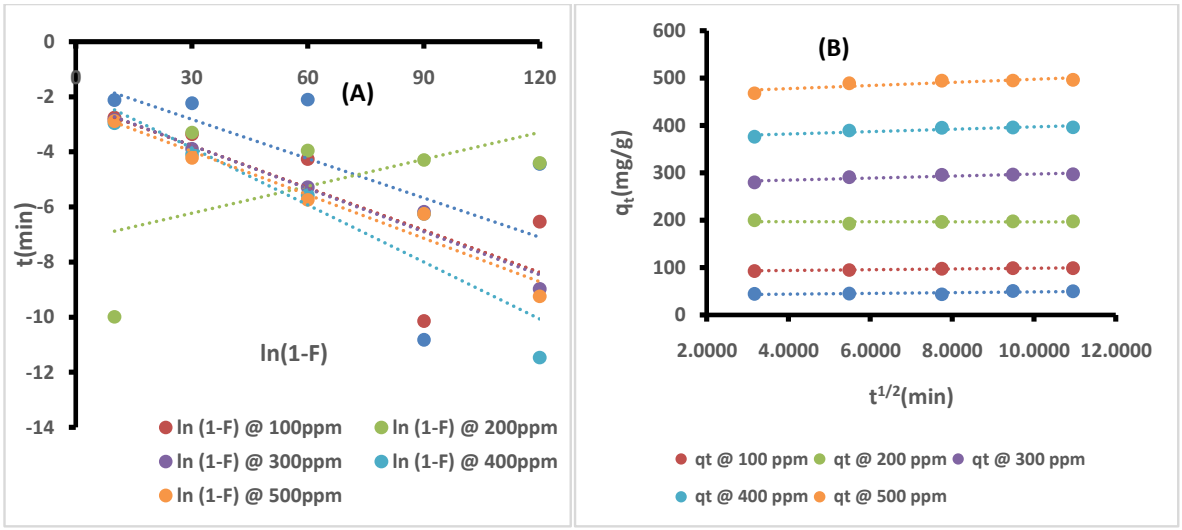


Figs. 3 (A) liquid film diffusion (B) Intraparticle diffusion for Adsorption of RhB onto B-nZVI

Table 1: Kinetic models parameters at different concentrations

| **Kinetics Models** | **Evaluated Parameters** | | | | |
|---|---|---|---|---|---|
| ***Pseudo first-order*** | **100 ppm** | **200 ppm** | **300 ppm** | **400 ppm** | **500 ppm** |
| $q_e$, *exp (mg/g)* | 98.65 | 199.85 | 296.8 | 396.31 | 496 |
| $q_e$, *cal (mg/g)* | 10.598 | 6.689 | 32.891 | 66.893 | 44.921 |
| $k_1(min^{-1})$ | -0.0512 | -0.0325 | -0.0521 | -0.069 | -0.0526 |
| $h_1$ *(mg/g/min)* | -0.5426 | -0.2174 | -1.7136 | -4.616 | -2.363 |
| $R^2$ | 0.5703 | 0.2829 | 0.9636 | 0.8739 | 0.9501 |
| *SSE* | 7753.15 | 37311.17 | 69647.96 | 108515.6 | 203472.3 |
| $\chi^2$ | 731.57 | 5577.99 | 2117.54 | 1622.23 | 4529.56 |
| ***Pseudo Second-order*** | | | | | |
| $q_e$, *exp (mg/g)* | 98.65 | 199.85 | 296.8 | 396.31 | 496 |
| $q_e$, *cal (mg/g)* | 99 | 196.08 | 303.03 | 400 | 500 |
| $k_2$ *(g/mg/min)* | 0.0096 | 0.0137 | 0.0045 | 0.0042 | 0.0033 |
| $h_2$ *(mg/g/min)* | 94.34 | 526.316 | 416.67 | 666.67 | 833.33 |
| $R^2$ | 1 | 0.999 | 1 | 1 | 1 |
| *SSE* | 0.1225 | 14.2129 | 38.8129 | 13.6161 | 16 |
| $\chi^2$ | 0.00124 | 0.0725 | 0.1281 | 0.034 | 0.032 |

Table 2: Mechanism model calculated values at different concentrations

| Mechanism Models | parameters | | | | |
|---|---|---|---|---|---|
| **Liquid film Diffusion** | **100 ppm** | **200 ppm** | **300 ppm** | **400 ppm** | **500 ppm** |
| $q_e$, *exp (mg/g)* | 98.65 | 199.85 | 296.8 | 396.31 | 496 |
| C | -2.2309 | -7.198 | -2.1999 | -1.7791 | -2.4017 |
| $R^2$ | 0.5703 | 0.2829 | 0.9636 | 0.8739 | 0.9501 |
| **Intraparticle Diffusion** | | | | | |
| K | 2.82 | -0.0498 | 2.1294 | 2.5001 | 3.2989 |
| C | 90.356 | 196.91 | 275.99 | 371.98 | 464.15 |
| $R^2$ | 0.9396 | 0.0033 | 0.8345 | 0.8194 | 0.7742 |

### 3.3: Thermodynamic Studies

One of the important parameters in adsorption studies is temperature. Extensive thermodynamics studies were carried out by varying temperature of the medium at different concentrations. Result obtained (Fig 4 and Table3) showed that uptake of RhB by BC-nZVI is temperature dependent. Increase in temperature increases the collision coefficient, rate of bombardment and kinetic energy of RhB molecules. Initially at the beginning of the uptake process, quantity adsorbed increased from 94.52 mg/g to 454.81 mg/g at 298 K until equilibrium was reached. Further increase in temperature did not record remarkable increase compared to quantity adsorbed at room temperature. This could be due to saturation of the active site and increase in mass transfer resistance [12-13]. Thus attribute of exothermic process is exhibited.

Fig 6 displays the thermodynamics graph from the linear plot of Van't Hoff equation (In Kc versus 1/T). Standard enthalpy, entropy and Gibb's free energy evaluated values are presented in Table 3. Negative values of $\Delta H^o$ confirmed exothermic process with fair degree randomness ($\Delta S^o$). Negative values of $\Delta G^o$ give assurance of the occurrence of the adsorption process confirming the viability and extemporaneity of the uptake of RhB using BC-nZVI [15, 21,23]

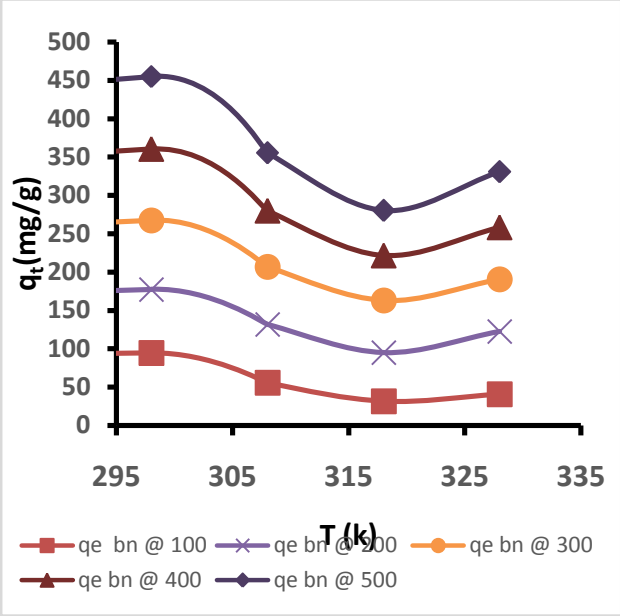


Fig. 4: Effect of Temperature on uptake of RhB onto BC-nZVI nto BC-nZVI

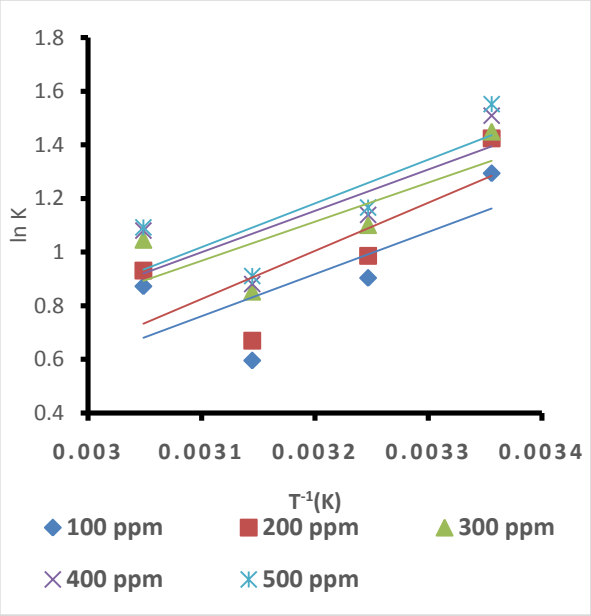


Fig. 5: Thermodynamics plot of RhB onto BC-nZVI

Table 3: Evaluated Thermodynamics parameters

| Concentration | T/K | ΔG Jmol$^{-1}$ | ΔS Jmol$^{-1}$K$^{-1}$ | ΔH Jmol$^{-1}$ |
|---|---|---|---|---|
| 100 pm | 298 | -3205.36 | -34.2445 | -1574.1 |
| | 308 | -2313.25 | | |
| | 318 | -1575.56 | | |
| | 328 | -2381.26 | | |
| 200 ppm | | | -39.4815 | -1797.9 |
| | 298 | -3528.98 | | |
| | 308 | -2523.78 | | |
| | 318 | -1768.96 | | |
| | 328 | -2539.4 | | |
| 300 ppm | | | -29.597 | -1460.5 |
| | 298 | -3592.35 | | |
| | 308 | -2817.84 | | |
| | 318 | -2253.47 | | |
| | 328 | -2851.82 | | |
| 400 ppm | | | -31.4984 | -1544.6 |
| | 298 | -3739.73 | | |
| | 308 | -2916.83 | | |
| | 318 | -2328 | | |
| | 328 | -2946.9 | | |
| 500 ppm | | | -33.6576 | -1634.5 |
| | 298 | -3846.93 | | |
| | 308 | -2985.97 | | |
| | 318 | -2409.25 | | |
| | 328 | -2977.6 | | |

### 3.4 Post Adsorption FTIR Spectroscopy

Figs 6(A & B) show the FTIR spectra of BC-nZVI and RhB-loaded- BC-nZVI. The corresponding FTIR assignment of peaks of BC-nZVI are as stated: the peaks between 3859.56 – 3118.90 $cm^{-1}$ are for corresponding to O–H stretching, 2360.95 $cm^{-1}$ and 2117.84 are characteristic of C-H stretching vibration band arising from the medium of storage, absolute ethanol before analysis. 1649 $cm^{-1}$ corresponds to H-O-H, 1269 $cm^{-1}$ to P=O, 1002.98 $cm^{-1}$ to SiO, 914.26 $cm^{-1}$ to Al–O, between 790 – 692 $cm^{-1}$ is Ca–O. The signals at 692.47 $cm^{-1}$, 534.3 $cm^{-1}$, 466.79 $cm^{-1}$ correspond to core shell Fe–O stretching [24]. However, it was observed that after adsorption, there was a decrease in the intensity of peaks of Fe–O, Si-O and Al–O while a broad OH band being introduced arose from the RhB solution.

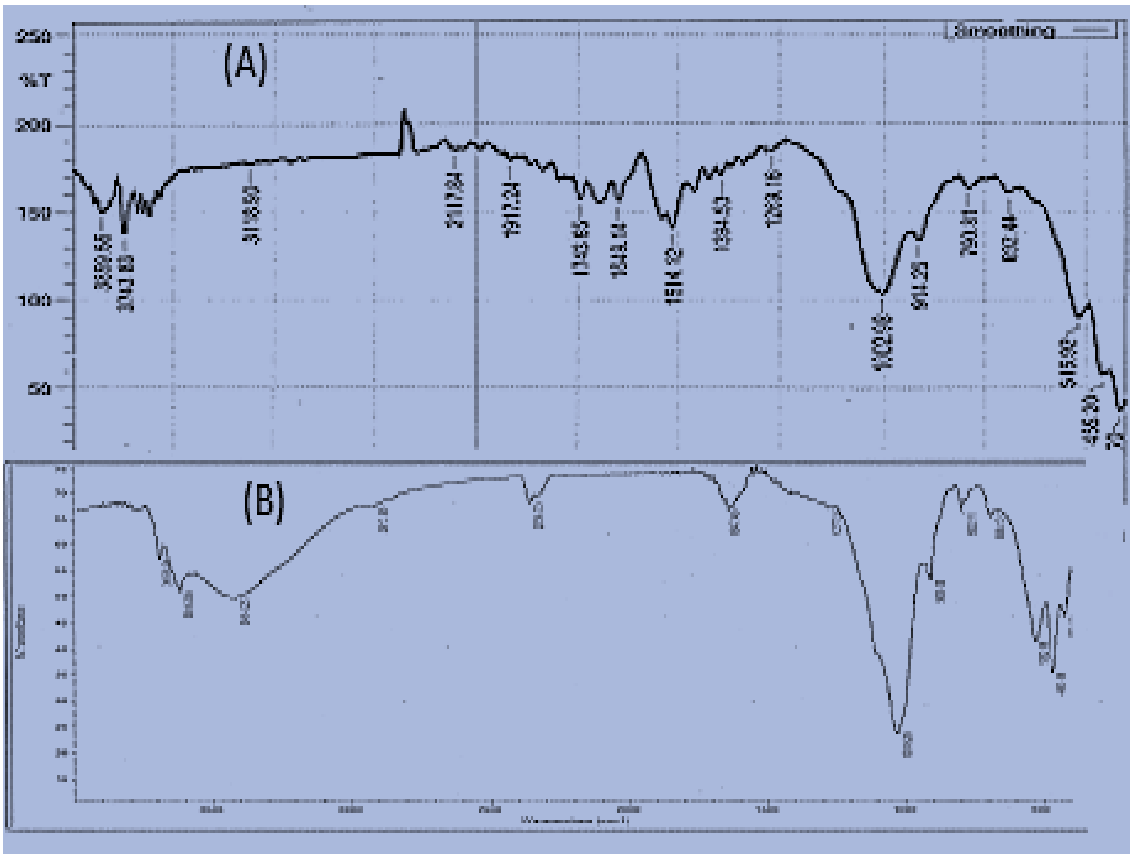


Fig. 6: (A) FTIR spectrum of BC-nZVI before adsorption (B) FTIR of BC-nZVI-RhB loaded after adsorption

### 4. Conclusion

This study examined the preparation of novel nanoscale Bentonite clay supported iron nanocomposite via chemical reduction using a single pot system. This study shows that uptake of RhB depend on concentration, contact time and temperature. Better percentage removal efficiency was obtained at room temperature. Pseudo second-order and liquid film diffusion better described kinetics and mechanism models. The correlation coefficients greater than 0.9 at higher concentration confirm the dominance of liquid film diffusion mechanism.

Feasibility, exothermic nature and randomness of RhB adsorption onto BC-nZVI were confirmed from thermodynamic studies. The FTIR gave information about involvement of the functional group and molecular environment of the nano-adsorbents before and after adsorption. It can therefore be concluded based on this research that the bentonite supported iron nano particles is a promising and efficient adsorbents which can be recommended to the industries for the treatment of their industrial effluents.

**Acknowledgement**
Enabling environment and facilities provided by the Management of Landmark University is highly appreciated

**References**

[1] Dos Santos, A.B., Cervantes F.J. and Lier J.B., (2007) "Review paper on the current technologies for decolourisation of textile wastewaters: perspectives for anaerobic biotechnology" Bioresource Technology, 77(3);247-255.
[2] Cousto S.R., (2009) "Dye removal by immobilized fungi" Biotechnology Advances27(3); 227-235.
[3] Dada, A. O., Adekola, F. A. and Odebunmi, E. O. (2017[a]). Kinetics, Mechanism, Isotherm and Thermodynamic Studies of Liquid Phase Adsorption of $Pb^{2+}$ onto Wood Activated Carbon Supported Zerovalent Iron (WAC-ZVI) Nanocomposite. *Cogent Chemistry Journal*. 3: 1351653, pg 1- 20.DOI: http://doi.org/10.1080/23312009.2017.1351653
[4] Lanciotti E., Galli S., Limberti A., Givannelli l., (2004) "Ecotoxicological evaluation of wastewater treatment plant effluent discharge: A case study in Parto (Italy)" Ann Ig, 16(1);549-580.
[5] Inyinbor, A. A., Adekola, F. A. and Olatunji, G. A. (2016). Kinetic and thermodynamic modeling of liquid phase adsorption of Rhodamine B dye onto Raphia hookerie fruit epicarp; Water Resources and Industry, Vol **15**, pg 14 –27
[6] Dada, A.O., Olalekan, A.P., Olatunya, A.M., and Dada, O. 2012. "Langmuir, Freundlich, Temkin and Dubinin–Radushkevich Isotherms Studies of Equilibrium Sorption of $Zn^{2+}$ unto Phosphoric Acid Modified Rice Husk". *Journal of Applied Chemistry* 3(2): 38-45
[7] Dada, A. O., Ojediran, J.O, Olalekan, A. P., 2013. Sorption of $Pb^{2+}$ from Aqueous Solution unto Modified Rice Husk: Isotherms Studies. Adv Phy Chem.2013, http://dx.doi.org/10.1155 /2013/842425
[8] Gupta, V.K and Nayak, A., 2012. Cadmium removal and recovery from aqueous solutions by novel adsorbent prepared from orange peel and $Fe_2O_3$ nanoparticles. *Chem. Engg. J.* 180, 81–90
[9] Xu, C., Wu, H., Gu, F. L. (2014). Efficient adsorption and photocatalytic degradation of RhodamineBunder visible light irradiation over BiOBr/montmorillonitecomposites ,*Journal of Hazardous Materials***275**, 185–192
[10] Singha, K. P., Gupta, S., Singha, A. K and Sinha, S. (2010). Experimental design and response surface modeling for optimization of Rhodamine B removal from water by magnetic nanocomposite, *Chemical Engineering Journal***165**, 151–160
[11] Motaharia, F., Mozdianfard, M. R., Salavati-Niasari, M. (2015). Synthesis and adsorption studies of NiO nanoparticles in the presence of $H_2$acacen ligand for removing Rhodamine B in wastewater treatment. *Process Safety and Environmental Protection*, **93**, 282–292
[12] Dada, A. O., Adekola, F.A., and Odebunmi, E.O. (2016[a]). "Kinetics and equilibrium models for Sorption of Cu(II) onto a Novel Manganese Nano-adsorbent". *Journal of Dispersion Science and Technology*, 37(1): 119 – 133
[13] Dada, A. O., Latona, D.F., Ojediran, J.O, and Osasuwa, N.O. (2016[b]). "Adsorption of Cu(II) onto Bamboo Supported Manganese (BS-Mn) nanocomposite: effect of operational parameters, kinetic, isotherms, and thermodynamic studies". *Journal of Applied Science Environmental Management,* 20(2): 404 – 422.
[14] Dada, A. O., Adekola, F. A. and Odebunmi, E. O. (2017[b]). Liquid Phase Scavenging of Cd (II) and Cu (II) ions onto novel nanoscale zerovalent manganese (nZVMn): Equilibrium, Kinetic and Thermodynamic Studies. *Environmental Nanotechnology, Monitoring & Management (Elsevier): 8, 63–72: //dx.doi.org/10.1016/j.enmm.2017.05.001*

[15] Dada, A. O., Adekola, F. A. and Odebunmi, E. O. (2017[c]) Novel zerovalent manganese for removal of copper ions: Synthesis, Characterization and Adsorption studies. *Applied water Science*, **7**,1409–1427 Doi: 10.1007/s13201-015-0360-5

[16] Li, L., Liu, S., Zhu, T. (2010). Application of activated carbon derived from scrap tires for adsorption of Rhodamine B. *Journal of Environmental Sciences*, **22**(8), 1273 –1280

[17] Adekola, F. A., Abdus–Salam, N., Adegoke, H.I., Adesola, M.A., Adekeye, JID, 2012. Removal of Pb(II) from Aqueous Solution by Natural and Synthetic Calcites. *Bull. Chem. Soc. Ethiop.,* 26(2), 195-210

[18] Senturk, H.B., Ozdes, D., Duran C (2010). Biosorption of Rhodamine 6G from aqueous solutions onto almond shell (*Prunus dulcis*) as a low cost biosorbent. *Desalination* 252: 81 – 87

[19] Lu P., Hu X., Li Y., Zhang M, Liu X, He Y., Dong F., Fu M, Zhang Z., (2018). One-step preparation of a novel $SrCO_3$/g-$C_3N_4$ nano-composite and its application in selective adsorption of crystal violet, RSC Adv. 8, 6315 –6325.

[20] Ahmad, M.A., Puad, N.A.A., Bello, O.S., 2014. Kinetic, equilibrium and thermodynamic studies of synthetic dye removal using pomegranate peel activated carbon prepared by microwave-induced KOH activation. *Water Resources and Industry, 6, 18 - 25*

[21] Boparai, H.K., Meera, J., Dennis, M. O (2011) Kinetics and thermodynamics of Cadmium ion removal by adsorption onto nano zerovalent iron particles. J. Harzard. Mater, 186, 458 – 465Doi:10.1016/j.jhazmat.2010.11.029

[22] Igwe, JC; Abia, AA; Ibeh, CA (2008). Adsorption kinetics and intraparticulate diffusivities of Hg, As and Pb ions on unmodified and thiolated coconut fiber. Int. J. Environ. Sci. Technol. 5, 83–92.

[23] Doğan, M., Türkyilmaz, A., Alkan, M., Demirbaş, Ö., 2009. Adsorption of copper (II) ions onto sepiolite and electrokinetic properties. Desalin., 238: 257–270

[24] Chen Z-X, Jin X-Y, Chen Z, Megharaj M, Naidu R (2011)., Removal of methyl orange from aqueous solution using bentonite-supported nanoscale zero-valent iron. J. Colloid Interface Sci 363: 601–607